Charge transfer of O^{3+} ions with atomic hydrogen

J. G. Wang* and P. C. Stancil†
Department of Physics and Astronomy and the Center for Simulational Physics, The University of Georgia, Athens, Georgia, 30602-2451

A. R. Turner‡ and D. L. Cooper§
Department of Chemistry, University of Liverpool, Liverpool L69 7ZD, United Kingdom

(Received 9 August 2002; published 30 January 2003)

Charge transfer processes due to collisions of ground state $O^{3+}(2s^2 2p\ ^2P)$ ions with atomic hydrogen are investigated using the quantum-mechanical molecular-orbital close-coupling (MOCC) method. The MOCC calculations utilize *ab initio* adiabatic potentials and nonadiabatic radial and rotational coupling matrix elements obtained with the spin-coupled valence-bond approach. Total and state-selective cross sections and rate coefficients are presented. Comparison with existing experimental and theoretical data shows our results to be in better agreement with the measurements than the previous calculations, although problems with some of the state-selective measurements are noted. Our calculations demonstrate that rotational coupling is not important for the total cross section, but for state-selective cross sections, its relevance increases with energy. For the ratios of triplet to singlet cross sections, significant departures from a statistical value are found, generally in harmony with experiment.

DOI: 10.1103/PhysRevA.67.012710 PACS number(s): 34.50.−s, 34.20.Mq, 34.70.+e

I. INTRODUCTION

The charge transfer process

$$O^{3+}(2s^2 2p\ \ ^2P^o) + H(1s) \rightarrow O^{2+}(2s^2 2p3l\ \ ^{1,3}L_J) + H^+ \quad (1)$$

is of great significance in astrophysical environments as it can modify the intensities of lines arising from the Bowen fluorescence mechanism. This fluorescence mechanism was first suggested to explain the anomalous strengths of certain emission lines of O^{2+} and N^{2+} observed in the spectra of planetary nebulae [1,2]. These anomalous line strengths have also been observed in many other astrophysical enviroments including galactic x-ray sources [3], transient x-ray sources [4,5], and the optical counterparts of x-ray bursters [6].

The Bowen fluorescence mechanism involves the UV pumping of $O^{2+}(2s^2 2p3d\ ^3P_2^o) \leftarrow O^{2+}(2s^2 2p^2\ ^3P_2)$ by a He^+ resonance line. The process occurs due to a fortuitous coincidence in wavelength between a He^+ emission line and an O^{2+} absorption line. This is followed by emission to other triplet states of O^{2+}, with photons from one of the lines emitted in the triplet cascade being absorped by N^{2+}. The $O^{3+}(2s^2 2p) + H$ charge transfer collisions that populate states such as $O^{2+}(2s^2 2p3p\ ^3D_J)$ and $O^{2+}(2s^2 2p3s\ ^3P_J^o)$ modify the intensities of the O^{2+} emission lines that are also thought to be affected by the Bowen mechanism. Data for the charge transfer process are therefore crucial to the understanding and interpretation of these emission lines as well as the related N^{2+} emission lines in astrophysical enviroments. In order to assess the effect of the charge transfer process, reliable rate coefficients are needed for capture into specific fine-structure levels of triplet $O^{2+}(2s^2 2p3s)$ and $O^{2+}(2s^2 2p3p)$. The charge transfer process also populates singlet states such as $O^{2+}(2s^2 2p3p\ ^1P)$ that are not involved in the Bowen fluorescence mechanism, so it is necessary to treat $^1\Sigma^+$, $^3\Sigma^+$, $^1\Pi$, and $^3\Pi$ states at the fine-structure level and using all relevant couplings.

As this charge transfer process is of considerable interest, a number of previous studies have been undertaken. An approach to this problem was made by Dalgarno and coworkers [7–11] using the CISD (configuration-interaction, singles, doubles) method to compute the potential energy curves. It was not possible at that time to treat all of the molecular states of interest. The radial couplings were computed using a variant of the Hellman-Feynman theorem [7] that may provide inaccurate values. Fully quantal [9,10] scattering calculations were used to obtain state-selective cross sections. They concluded that only the $O^{2+}(2s^2 2p3s)$ and $O^{2+}(2s^2 2p3p)$ configurations are populated for collisional energies ranging from thermal up to 5000 eV/u, while capture to the $O^{2+}(2s^2 2p3d)$ was found not to be important. Later Gargaud *et al.* [12] used the model potential method. Although this method reproduces the asymptotic energies exactly, it is uncertain as to whether the smaller internuclear separation region is treated to a similar level of accuracy. Again, a fully quantal treatment was used for the scattering calculations. Those authors concluded that capture into the $O^{2+}(2s^2 2p3p\ ^1S)$ and $O^{2+}(2s^2 2p3p\ ^1D)$ states may be neglected as the crossings are diabatic for all practical purposes. But compared with the earlier work, their results differed by as much as an order of magnitude.

Numerous experimental studies have also been performed. Church and Holzscheiter [13] measured the total electron capture rate coefficient at 2.5×10^4 K in a Penning trap. Their result is in good agreement with the calculated value of Heil *et al.* [9], but the measurement had a relatively large error bar. Total SEC (single electron capture) cross sec-

*Electronic address: wangjg@physast.uga.edu
†Electronic address: stancil@physast.uga.edu
‡Present address: Department of Chemistry, University of Edinburgh, West Mains Road, Edinburgh EH9 3JJ, United Kingdom. Electronic address: Andrew.Turner@ed.ac.uk
§Electronic address: dlc@liv.ac.uk

tions were measured from 42 to 4915 eV/u by Phaneuf *et al.* [14] via charge-state analysis using a pulsed laser ion source with a time-of-flight electron collision apparatus. Recently, Havener *et al.* [15,16] improved the measurements with an ion-atom merged-beams technique with a 99.98% pure ground-state H or D beam produced by passing a 6- to 9-keV beam of H^- and D^- ions through the optical cavity of a laser. They obtained the total absolute SEC cross section for the energy range between 0.1 and 1000 eV/u. Their values showed a systematic discrepancy from calculated values over the entire energy range, especially for low energy, with the theoretical cross sections being 2–3 times larger than the measurements. Relative state-selective SEC cross sections were measured by Wilson *et al.* [17] using translational energy spectroscopy (TES) and showed that capture into the $O^{2+}(2s^2 2p 3s)$ channel dominates between 263 and 750 eV/u, which is consistent with the calculations of Gargaud *et al*. However, more recent measurements of the state-selective SEC cross sections between 45 and 752 eV/u by Beijers *et al.* [19] via photon emission spectroscopy (PES) did not reproduce the earlier results: SEC into both the $O^{2+}(2s^2 2p 3s)$ and $O^{2+}(2s^2 2p 3p)$ configurations was found to be important for energies down to around 100 eV/u and capture into the $O^{2+}(2s^2 2p 3p)$ channel dominated for lower energies. In order to resolve the discrepancies among the different theories and experiments, further theoretical and experimental investigations are required.

In this paper, charge transfer processes due to collisions of ground-state $O^{3+}(2s^2 2p\ ^2P)$ ions with atomic hydrogen are investigated using the quantum-mechanical molecular-orbital close-coupling (MOCC) method at the *LS* level of resolution. The MOCC calculations utilize *ab initio* adiabatic potentials and nonadiabatic radial and rotational coupling matrix elements obtained with the spin-coupled valence-bond (SVCB) approach. Total and state-selective cross sections are calculated and compared with the available theoretical and experimental data. Total and state-selective rate coefficients are also presented. Section II describes the molecular potential and coupling data utilized in the MOCC calculations, while Sec. III discusses the scattering calculation approach. Section IV presents the results of the scattering calculations including comparisons of total and state-selective cross sections and rate coefficients with other theories and experiments, while Sec. V briefly gives a summary of the work. Atomic units are used throughout unless otherwise noted.

II. ELECTRONIC STRUCTURE CALCULATIONS

The adiabatic potential energy curves, nonadiabatic radial couplings, and rotational couplings for the four symmetries of interest ($^1\Sigma^+$, $^1\Pi$, $^3\Sigma^+$, and $^3\Pi$) were obtained using the SCVB method (see, for example, Cooper *et al.* [20]). This is a fully flexible *ab initio* technique and, as such, we expect the molecular region to be described with much the same accuracy as in the asymptotic separated-atom limit.

We adopted a Dunning correlation-consistent basis set of quintuple-ζ quality for O-H consisting of $(14s8p4d3f)/(8s4p3d)$ Cartesian Gaussian type orbitals generally contracted to $[6s5p4d3f]/[5s4p3d]$. This set was augmented by two diffuse, even-tempered basis functions on oxygen, one *s*-type function and one *p*-type function. The oxygen core electrons ($1s^2$) were assumed to have little or no effect on the charge transfer process and so they were accommodated in appropriate orthogonal natural orbitals taken from a state-averaged multiconfiguration self-consistent field calculation on triplet atomic O^{2+}. The remaining four valence electrons were described by fully optimized, singly occupied, nonorthogonal orbitals from within a spin-coupled calculation that was designed to give the $^3\Sigma^-$ ground-state configuration $[O^{2+}(2s^2 2p^2) + H^+$, asymptotically]. This symmetry was chosen so as to ensure that the virtuals would not be biased to any particular molecular symmetry under investigation. At convergence, a set or ''stack'' of virtual orbitals was generated for each valence electron. A total of 20 virtual orbitals was selected for the SCVB expansions; the first and second stacks [$\phi_{occ} \approx O^{2+}(2s)$, $O^{2+}(2s')$] together contributed four σ virtuals, two pairs of π virtuals, and one pair of δ virtuals, while the third and fourth stacks [$\phi_{occ} \approx O^{2+}(2p_{\pi^+})$, $O^{2+}(2p_{\pi^-})$] together contributed four σ virtuals, two pairs of π virtuals, and one pair of δ virtuals. To improve the description of the entrance channels, a set of nine orthogonal natural orbitals $(3s, 3p_\sigma, 3p_{\pi\pm}, 3d_\sigma, 3d_{\pi\pm}, 3d_{\delta\pm})$ was imported from a MO-based CISD calculation on atomic O^{3+}.

Separate SCVB (nonorthogonal CI) expansions were then performed for each of the four molecular symmetries, using this single set of virtuals. The SCVB configuration space for each case was constructed by performing all single and double vertical excitations, along with singly ionic excitations, that yielded configurations of the correct symmetry. A vertical excitation is the replacement of an occupied orbital by a virtual from its own stack and a singly ionic excitation is the double occupancy of a single virtual by means of a single vertical excitation along with one cross excitation. The reference space consisted of the spin-coupled configuration and the dominant configuration of each excited state. The dominant configuration for each excited state was found to correspond directly with the appropriate asymptotic separated-atom configuration. Additional selected excitations to the imported natural orbitals were also performed. For the $^1\Sigma^+$ states, this procedure generated 562 spatial configurations (670 symmetry-adapted VB structures), for the $^1\Pi$ states, 536 spatial configurations (741 symmetry adapted VB structures), for the $^3\Sigma^+$ states, 399 spatial configurations (496 symmetry-adapted VB structures), and for the $^3\Pi$ states, 410 spatial configurations (886 symmetry-adapted VB structures). Additional details of the SCVB calculations are given by Turner [21].

A comparison of our calculated asymptotic energy separations with experimental values and with the calculated values of Butler *et al.* [7] is shown in Table I. The maximum deviation of the current results from the experimental energy separations is in the $1\ ^3\Sigma^+$ state, with an error of just 0.16 eV; most of the other energy separations are reproduced to better than 0.1 eV. In general, our asymptotic separations are consistently better than those of the previous study of Butler *et al.*, especially in reproducing the degeneracies between appropriate Σ^+ and Π states. All of the required degenera-

TABLE I. Asymptotic separated-atom energies for the states of OH^{3+}.

Molecular states	Asymptotic atomic states	Energy (eV)		
		Theory [a]	Theory [b]	Expt. [c]
$1\ ^3\Sigma^+$	$O^{2+}(2s^2 2p3s\ ^3P^o)+H^+$	−8.01	−8.12	−8.17
$1\ ^3\Pi$	$O^{2+}(2s^2 2p3s\ ^3P^o)+H^+$	−8.01	−7.99	−8.17
$1\ ^1\Sigma^+$	$O^{2+}(2s^2 2p3s\ ^1P^o)+H^+$	−7.55	−7.40	−7.48
$1\ ^1\Pi$	$O^{2+}(2s^2 2p3s\ ^1P^o)+H^+$	−7.54	−7.30	−7.48
$2\ ^3\Pi$	$O^{2+}(2p^4\ ^3P)+H^+$	−6.14		−6.14
$2\ ^1\Pi$	$O^{2+}(2s^2 2p3p\ ^1P)+H^+$	−5.32	−4.93	−5.26
$2\ ^3\Sigma^+$	$O^{2+}(2s^2 2p3p\ ^3D)+H^+$	−4.83	−4.92	−4.88
$3\ ^3\Pi$	$O^{2+}(2s^2 2p3p\ ^3D)+H^+$	−4.87	−4.64	−4.88
$3\ ^3\Sigma^+$	$O^{2+}(2s^2 2p3p\ ^3S)+H^+$	−4.30	−4.52	−4.44
$2\ ^1\Sigma^+$	$O^{2+}(2p^4\ ^1D)+H^+$	−4.38		−4.35
$3\ ^1\Pi$	$O^{2+}(2p^4\ ^1D)+H^+$	−4.40		−4.35
$4\ ^3\Pi$	$O^{2+}(2s^2 2p3p\ ^3P)+H^+$	−4.10		−4.10
$3\ ^1\Sigma^+$	$O^{2+}(2s^2 2p3p\ ^1D)+H^+$	−3.35		−3.33
$4\ ^1\Pi$	$O^{2+}(2s^2 2p3p\ ^1D)+H^+$	−3.30		−3.33
$4\ ^1\Sigma^+$	$O^{2+}(2s^2 2p3p\ ^1S)+H^+$	−2.36		−2.43
$5\ ^1\Sigma^+$	$O^{2+}(2s^2 2p\ ^2P^o)+H(1s\ ^2S)$	0	0	0
$4\ ^3\Sigma^+$	$O^{2+}(2s^2 2p\ ^2P^o)+H(1s\ ^2S)$	0	0	0
$5\ ^1\Pi$	$O^{2+}(2s^2 2p\ ^2P^o)+H(1s\ ^2S)$	0	0	0
$5\ ^3\Pi$	$O^{2+}(2s^2 2p\ ^2P^o)+H(1s\ ^2S)$	0	0	0

[a]This work.
[b]Butler *et al.* [7].
[c]NIST Atomic Spectra Database [40].

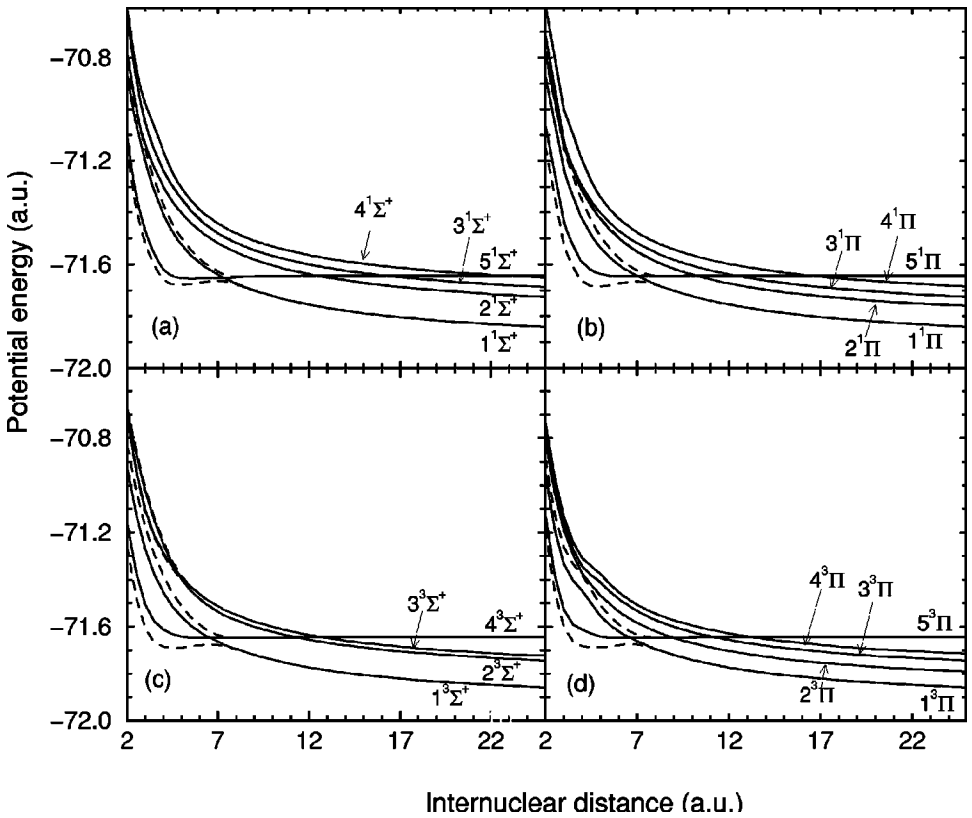

FIG. 1. The adiabatic (long dashed line) and diagonal diabatic (solid line) potential energies for the OH^{3+} system as a function of internuclear distance *R*.

TABLE II. Avoided crossing distances R_x and energy separations $\Delta U(R_x)$ for the adiabatic states of OH^{3+} (adiabatic labels).

Molecular state	Final O^{2+} state	$R_x(a_0)$		ΔU (eV)	
		Theory [a]	Theory [b]	Theory [a]	Theory [b]
$1\ ^1\Sigma^+-2\ ^1\Sigma^+$	$2p3s\ ^1P^o$	7.54	7.6	0.647	0.968
$2\ ^1\Sigma^+-3\ ^1\Sigma^+$	$2p^4\ ^1D$	12.49		0.001	
$3\ ^1\Sigma^+-4\ ^1\Sigma^+$	$2p3p\ ^1D$	16.23	16.3	0.003	0.001
$4\ ^1\Sigma^+-5\ ^1\Sigma^+$	$2p3p\ ^1S$	23.09	22.3	0.001	0.000
$1\ ^1\Pi-2\ ^1\Pi$	$2p3s\ ^1P^o$	7.73	7.6	0.870	0.968
$2\ ^1\Pi-3\ ^1\Pi$	$2p3p\ ^1P$	10.23	10.3	0.066	0.088
$3\ ^1\Pi-4\ ^1\Pi$	$2p^4\ ^1D$	12.40		0.003	
$4\ ^1\Pi-5\ ^1\Pi$	$2p3p\ ^1D$	16.49	16.3	0.001	0.001
$1\ ^3\Sigma^+-2\ ^3\Sigma^+$	$2p3s\ ^3P^o$	7.18	7.1	1.078	1.117
$2\ ^3\Sigma^+-3\ ^3\Sigma^+$	$2p3p\ ^3D$	11.34	11.1	0.038	0.062
$3\ ^3\Sigma^+-4\ ^3\Sigma^+$	$2p3p\ ^3S$	12.76	12.2	0.012	0.020
$1\ ^3\Pi-2\ ^3\Pi$	$2p3s\ ^3P^o$	7.27	7.1	1.077	1.177
$2\ ^3\Pi-3\ ^3\Pi$	$2p^4\ ^3P$	8.97		0.007	
$3\ ^3\Pi-4\ ^3\Pi$	$2p3p\ ^3D$	11.22	11.1	0.034	0.054
$4\ ^3\Pi-5\ ^3\Pi$	$2p3p\ ^3P$	13.27	13.2	0.012	0.011

[a]This work.

[b]Gargaud *et al.* [12].

cies between asymptotic states were reproduced to better than 0.05 eV and the maximum deviation in the absolute energies between the four entrance channels is just 0.02 eV.

The resulting adiabatic potential energy curves over the range $R=(2-25)a_0$ are shown for the $^1\Sigma^+$, $^1\Pi$, $^3\Sigma^+$, and $^3\Pi$ states in Fig. 1. The avoided crossing distances R_x and the corresponding energy separations $\Delta U(R_x)$ are listed in Table II. For the $^1\Sigma^+$, $^1\Pi$, and $^3\Pi$ symmetries, the avoided crossings between the $O^{2+}(2p^4)+H^+$ potentials and the $O^{3+}(2s^22p)+H(1s)$ potentials (i.e., the $2\ ^1\Sigma^+-3\ ^1\Sigma^+$, $3\ ^1\Pi-4\ ^1\Pi$, and $2\ ^3\Pi-3\ ^3\Pi$ avoided crossings) are extremely sharp with small energy separations. As a result, the nonadiabatic transition probabilities will be practically unity at all the collision energies of interest, and these avoided crossings can be accurately treated as if they are diabatic crossings (thus excluding the $2p^4$ channels from the MOCC calculations). Two other avoided crossings were treated diabatically due to their sharpness: the $4\ ^1\Sigma^+-5\ ^1\Sigma^+$ avoided crossing at $23.01a_0$ (leading to the exclusion of the $2p3p\ ^1S$ channel from the MOCC cross sections) and the $4\ ^1\Pi-5\ ^1\Pi$ avoided crossing at $\sim 16.49a_0$ (leading to the exclusion of the $2p3p\ ^1D$ channel). None of the channels excluded from the MOCC calculations are thought to contribute significantly to the charge transfer cross sections at the usual low collision energies of astrophysical interest.

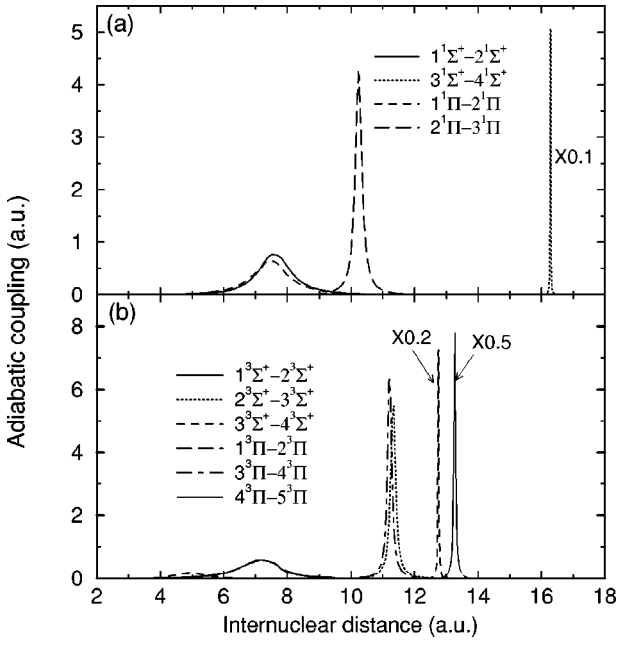

FIG. 2. Computed nonadiabatic radial couplings for the OH^{3+} system as a function of internuclear distance R. (a) $^1\Sigma^+$ and $^1\Pi$; (b) $^3\Sigma^+$ and $^3\Pi$.

Comparison of the current SCVB R_x and $\Delta U(R_x)$ is made with those obtained by Gargaud *et al.* [12] in Table II. Differences between R_x are less than $0.25a_0$ except for the $4\ ^1\Sigma^+-5\ ^1\Sigma^+$ and $3\ ^3\Sigma^+-4\ ^3\Sigma^+$ avoided crossings. More important, however, are the energy splittings at R_x. For all of the dominant capture channels, the splittings calculated with the model potential method by Gargaud *et al.* are somewhat larger than the current results. The differences are important as the electron capture cross sections are known to depend sensitively on ΔU as will be shown below.

The computed radial couplings between the adiabatic states (matrix elements of $\partial/\partial R$) are illustrated in Fig. 2. The couplings were calculated using the central difference approximation with the electronic coordinate origin at the center of mass. The peaks corresponding to the avoided cross-

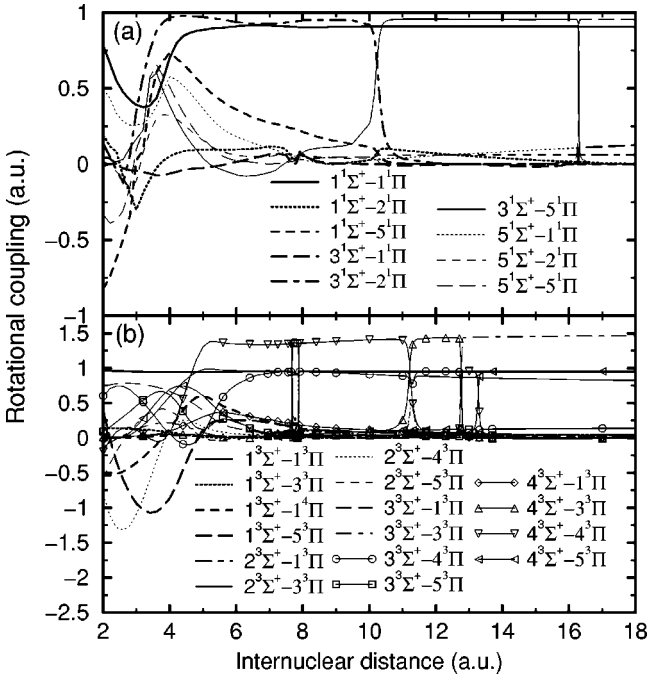

FIG. 3. Rotational couplings for the OH^{3+} system as a function of internuclear distance *R*. (a) Singlets; (b) triplets.

ings are smooth, well defined, and centered on, or near, the positions of the avoided crossings. The couplings between nonadjacent states are much smaller than those between adjacent states and were found to have a negligible effect on the form of the *p*-diabatic potential energy matrices. As a consequence, they could be reset to zero for all internuclear separations. Using the nonadiabatic radial couplings, we transformed each set of molecular data to the *p*-diabatic representation by a unitary transformation to eliminate first-order derivatives [9,22]. The diagonal elements of the resulting *p*-diabatic potential energy matrices are displayed in Fig. 1. All of the elements of the *p*-diabatic potential energy matrices vary smoothly over the entire range of internuclear separations.

Rotational couplings between the adiabatic states (matrix elements of the form $\langle\Psi_i|iL_y|\Psi_j\rangle$) have been computed using the Löwdin formula [23] for matrix elements between nonorthogonal determinants constructed from nonorthogonal spin orbitals. These couplings drive transitions between states of the same spin, but of different spatial symmetry. The couplings between the $^1\Sigma^+$ and $^1\Pi$ states are shown in Fig. 3(a), while the couplings between $^3\Sigma^+$ and $^3\Pi$ states are shown in Fig. 3(b). We neglect rotational coupling to $^{1,3}\Sigma^-$ and $^{1,3}\Delta$ states.

III. SCATTERING THEORY

The quantum-mechanical MOCC method, which we only briefly discuss here, has been described thoroughly in the literature [22,24]. It involves solving a coupled set of second-order differential equations. Its solutions are the expansion coefficients, or scattering amplitudes, of the total system wave function expanded over a truncated set of molecular eigenfunctions. In the adiabatic representation, transitions between channels are driven by elements (radial A^R and rotational A^θ) of the vector potential $A(\vec{R})$, where $\vec{R}$ is the internuclear distance vector. Since the adiabatic description contains first-order derivatives, it is numerically convenient to make a unitary transformation [9,22], which is affected by the radial portion of $A(\vec{R})$, to a diabatic representation

$$U(R)=W(R)[V(R)-P(R)]W^{-1}(R) \tag{2}$$

where $U(R)$ is the diabatic potential matrix, $V(R)$ is the diagonal adiabatic potential, $W(R)$ is a unitary transformation matrix, and the components of the rotational coupling matrix are

$$P_{mn}=\pm\frac{1}{\mu R^2}[(J\mp\lambda_m)(J\pm\lambda_m+1)]^{1/2}A^\theta_{mn}\delta(\lambda_m,\lambda_n\pm1) \tag{3}$$

(e.g., [25]), where μ is the reduced mass, J is the total angular momentum, and λ is the component of electronic angular momentum along the internuclear axis.

The electron capture cross section from initial channel *i* to final channel *j* is given by

$$\sigma_{i\to j}=\frac{\pi}{k_i^2}\sum_J(2J+1)|S_J|^2_{i,j} \tag{4}$$

where the *S* matrix is

$$S_J=[I+iK_J]^{-1}[I-iK_J], \tag{5}$$

and k_i is the initial momentum. The *K* matrix is obtained from the scattering amplitude after a partial-wave decomposition (e.g., [22]) and *I* is the identity matrix. The coupled scattering equations are integrated using the log-derivative method of Johnson [26]. In this work, electron translation factors (ETFs; e.g., [24]), which are often used to modify the molecular eigenfunctions to remove asymptotic couplings between atomic states that are connected by dipole transitions, are not included. The influence of ETFs is expected to be important for $E>1$–5 keV/u (e.g., [27,28]), which is beyond the maximum calculated energy of this work.

IV. RESULTS AND DISCUSSION

The total and state-selective cross sections[1] are calculated with and without rotational couplings. Without rotational coupling, the calculations are performed according to the symmetry $^1\Sigma^+$ (three-channel MOCC), $^3\Sigma^+$ (four-channel MOCC), $^1\Pi$ (three-channel MOCC), and $^3\Pi$ (four-channel MOCC). With rotational coupling, there are interactions be-

[1]Complete numerical cross section and rate coefficient data can be obtained from the authors or from the ORNL-UGA Charge Transfer Database for Astrophysics webpage URL: cfadc.phy.ornl.gov/astro/ps/data.

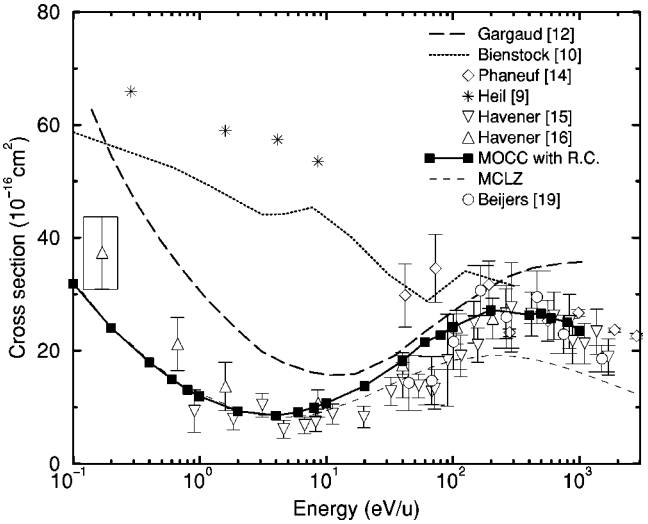

FIG. 4. Total SEC cross sections for $O^{3+}+H$. Theory: present calculation with rotational coupling (thick — with filled squares), Gargaud *et al.* [12] (thick - -), Bienstock *et al.* [10] (thick $\cdots$), Heil *et al.* [9] ($\star$), MCLZ (thin - -). Experiment: Phaneuf *et al.* [14] (open diamonds), Havener *et al.* [15] (open triangles down), Havener *et al.* [16] (open triangles up), ''corrected'' Beijers *et al.* [19] (open circles).

tween states with the same spin angular momentum so that two sets of calculations are performed, one for the singlet states $^1\Sigma^+$ and $^1\Pi$ (six-channel MOCC) and one for the triplet states $^3\Sigma^+$ and $^3\Pi$ (eight-channel MOCC). The total and state-selective cross sections are obtained according to the statistical weights of the different symmetries.

A. Total cross sections

Figure 4 shows the total MOCC cross section for the collisional energy range between 0.1 and 1000 eV/u compared to the available calculations and measurements. At low collision energies (<1 eV/u), the cross sections display the typical Langevin $E^{-1/2}$ behavior. At about 4 eV/u, the present MOCC total cross section reaches a local minimum, and then increases slowly to a local maximum at about 200 eV/u. When the collisional energy $E>200$ eV/u, the cross section decreases slowly with increasing energy. When $E<10$ eV/u, the differences between the current total MOCC cross sections with and without rotational coupling are small ($<4\%$), demonstrating that rotational coupling is not important at low energy. With increasing energy, rotational coupling becomes more important with the differences of the cross sections increasing, but only slightly. At about 100 eV/u, the differences reach a maximum, where the cross section including rotational coupling is 6% higher than that without rotational coupling. In general, for total cross sections, rotational coupling is not important in the energy region studied. Cross sections were also calculated with the multichannel Landau-Zener (MCLZ) method using empirical parameters [30,31]. At low energy ($E<10$ eV/u), the MCLZ cross section is in good agreement with the MOCC results. With increasing energy ($E>10$ eV/u), the accuracy of MCLZ method decreases, and by 400 eV/u, the MCLZ cross section is only about half of the MOCC result.

All of the previous calculations [9,10,12] are 2–5 times larger than the present MOCC results. Although all of the earlier results were obtained with the quantal MOCC method, the differences in the total cross sections probably can be attributed to the different molecular structure calculations.

For the collisional energy range $0.8\leqslant E\leqslant 1000$ eV/u, the present total MOCC cross section is in good agreement with Havener *et al.*'s measurement [15,16]. For $0.1\leqslant E<0.8$ eV/u, only two measured points exist, which are about 30% larger than our calculations. But, if the uncertainity in the beam energy due to an estimated energy spread of 0.1 eV/u at a collision energy of 0.1 eV/u [16] is considered, the current calculations fall just below the left corner of the uncertainty box of the 0.17 eV/u measurement. Havener *et al.* [16] proposed that a finite fraction of the O^{3+} ion beam might be in the $(2s2p^2\ ^4P)$ metastable state, possibly contributing, at least in part, to the discrepancy with previous calculations. However, using the MCLZ method with empirical parameters [30], we estimate the metastable charge transfer cross section to be slightly smaller than the ground-state cross section in this energy range. Therefore, metastable contamination of the ion beam does not appear to be significant enough to account for the discrepancy between the merged-beam measurements and the previous calculations or the minor differences with the current results for $0.1\leqslant E<0.8$ eV/u. Further, the local minimum near 5 eV/u in the experimental total cross section is only present in the current quantal MOCC results for the ground state, but not for the metastable state. This gives some additional evidence to suggest that the contribution from the metastable state is negligible, although the level of uncertainty is far greater in the MCLZ calculation as opposed to the MOCC results.

Another possibility for the low-energy discrepancy might be related to the fact that the measurements of Havener *et al.* [15,16] below 834 eV/u where made with a D beam. To test this, we made MOCC calculations for $O^{3+}+D$ for energies between 0.1 and 10 eV/u. As expected [16,29], the D cross section was found to be *smaller* than the cross sections for H, but only by about 3%. The kinematic isotope does not appear to be significant for this particular collision system, at least in regard to the total cross section.

For $E>40$ eV/u, a number of other experimental results are available including the measurement of Phaneuf *et al.* [14] which appears to overestimate the total cross section. In the Beijers *et al.* [19] experiment, PES of the product ions was used to determine absolute state-selective cross sections. In principle, if one could measure all of the emission from the dominant capture channels, then the total cross section could be obtained from the sum of the state-selective cross sections. However, only a portion of the transitions could be measured due to the limited wavelength window of their detector. Therefore, the state-selective cross sections are inferred from the measured emission cross sections in conjunction with spontaneous transition probability branching ratios. However, as will be discussed more fully in the next section, we found that the adopted branching ratios are not reliable

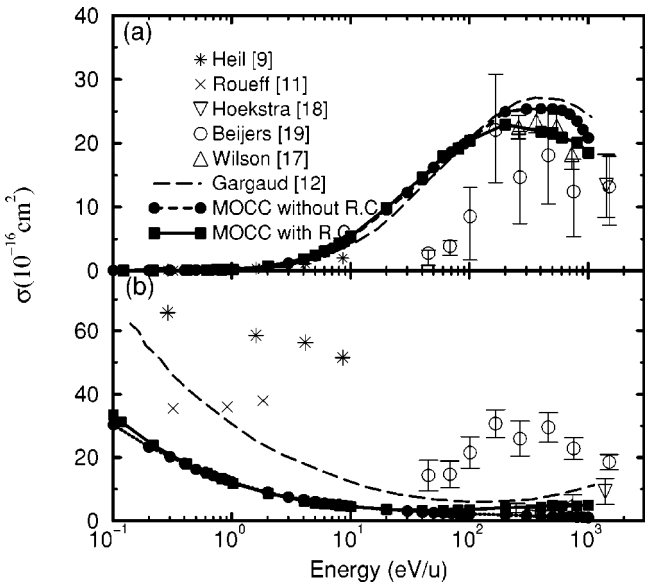

FIG. 5. State-selective cross sections. (a) Capture to state $O^{2+}(2p3s)$; (b) capture to state $O^{2+}(2p3p)$. Theory: present calculation with rotational coupling (thick — filled squares), present calculation without rotational coupling (thick ··· with filled squares), Gargaud *et al.* [12] (thick - -), Heil *et al.* [9] (⋆), Roueff and Dalgarno [11] (×). Experiment: ''corrected'' Beijers *et al.* [19] (open circles); Wilson *et al.* [17] (open triangles up); Hoekstra *et al.* [18] (open triangles down).

when compared with a critical compilation [32] resulting in errors of about 30%–50%, which translate into enhancements of 30%–100% for the cross sections. The ''corrected'' experimental data from the Beijers *et al.* [19] work are presented in Fig. 4. After these corrections are made, the present MOCC cross section is in good agreement with Beijers *et al.*'s data. It is unknown whether a similar problem exists in the measurements of Hoekstra *et al.* [18]. Over the whole energy range considered, the present MOCC calculations show the best agreement to date with the measurements.

B. State-selective cross sections

State-selective cross sections for capture to configurations $O^{2+}(2p3s)$ and $O^{2+}(2p3p)$ are shown in Fig. 5. In the low-energy regime, capture to $O^{2+}(2p3p)$ dominates. With increasing energy, capture to $O^{2+}(2p3s)$ becomes important; when $E>20$ eV/u, it begins to dominate over capture to $O^{2+}(2p3p)$. This is because capture to $O^{2+}(2p3s)$ occurs at intermediate avoided crossing distances $[\sim(7-8)a_0]$, while capture to $O^{2+}(2p3p)$ proceeds through long avoided crossing distances $[\sim 10-13a_0]$. Similar behaviors can be found in Gargaud *et al.*'s calculations [12] and the measurements of Wilson *et al.* [17].

Figure 5 also shows MOCC results with and without rotational coupling. At low energy (<40 eV/u), the cross sections with and without rotational coupling are similar; however, the differences increase with increasing energy. When $E=700$ eV/u, the cross section for capture to $O^{2+}(2p3s)$ decreases 25%, while the cross section for capture to $O^{2+}(2p3p)$ increases by a factor of 3 when rotational coupling is considered. Rotational coupling tends to decrease the larger cross section and increase the smaller one.

TABLE III. Wavelengths (λ) and branching ratios (BR) of cascade emission lines for $O^{2+}(2p3p\ ^3P,^3D)$.

	Upper state			
	$2p3p\ ^3P$		$2p3p\ ^3D$	
Lower state	λ (nm)	BR	λ (nm)	BR
$2s2p^3\ ^3S^o$	96.8 [a]	0.003 [a]		
	99.3 [b]	0.0036 [b]		
$2p3s\ ^3P^o$	304.1 [a]	0.531 [a]	376.2 [a]	0.509 [a]
	304.7 [b]	0.732 [b]	377.2 [b]	0.649 [b]
$2s2p^3\ ^3P^o$	63.3 [a]	0.064 [a]	65.9 [a]	0.318 [a]
	63.6 [b]	0.156 [b]	65.9 [b]	0.310 [b]
$2s2p^3\ ^3D^o$	55.4 [a]	0.401 [a]	57.4 [a]	0.173 [a]
	55.4 [b]	0.109 [b]	57.4 [b]	0.041 [b]

[a]Calculated from Wiese *et al.* [32].
[b]Beijers *et al.* [19].

Compared with other theoretical calculations for capture to $O^{2+}(2p3s)$, the present results are in agreement generally to within 50%. However, for capture to the $O^{2+}(2p3p)$, all of the previous calculations [9,11,12] appear to have overestimated the cross section, especially for energies <10 eV/u. This cross section is dominated by capture to $2p3p\ ^3D$ and Table II shows that the potential splittings $\Delta U(R_x)$ of Gargaud *et al.* are 60% larger than those calculated in this work, which likely accounts for the discrepancy. The difference in the $2p3p$ configuration cross section is responsible for the overestimation of the total cross sections in Fig. 4 as compared to the measurements of Havener *et al.* [15,16].

Three state-selective measurements are available for this collision system, which include the previously mentioned PES results of Hoekstra *et al.* [18] and Beijers *et al.* [19] as well as the TES experiment of Wilson *et al.* [17]. While absolute state-selective cross sections at the *LS* level can be inferred with the PES method (in this case $2p3s\ ^1P^0,^3P^0$; $2p3p\ ^3S,^3P,^3D$), only relative cross sections at the configuration level (i.e., $2p3s$ and $2p3p$) can be obtained via TES. However, there appear to be some difficulties with the reported PES results. As discussed above, the branching ratios adopted in Ref. [19] are inaccurate compared to those obtained from Wiese *et al.* [32], as shown in Table III. Using the new branching ratios, we corrected the data of Ref. [19] which resulted in increases of the cross sections by 30–100 %. Two other issues appear to complicate the measurements of Beijers *et al.* [19]: (i) a 12% metastable contamination of the oxygen ion beam and (ii) a partially dissociated (~70%) neutral H-H_2 target beam. Because some fraction of H_2 is present in the target beam, a PES measurement must first be made for a pure H_2 beam with the resulting spectrum subtracted from the composite H-H_2 spectrum. Beijers *et al.* [19] report significant cross section magnitudes for capture to all of the *LS* states except $2p3p\ ^3S$ following O^{3+} collisions with H_2. However, for collisions with ground-state O^{3+} the $2p3p\ ^3P,^3D$ capture

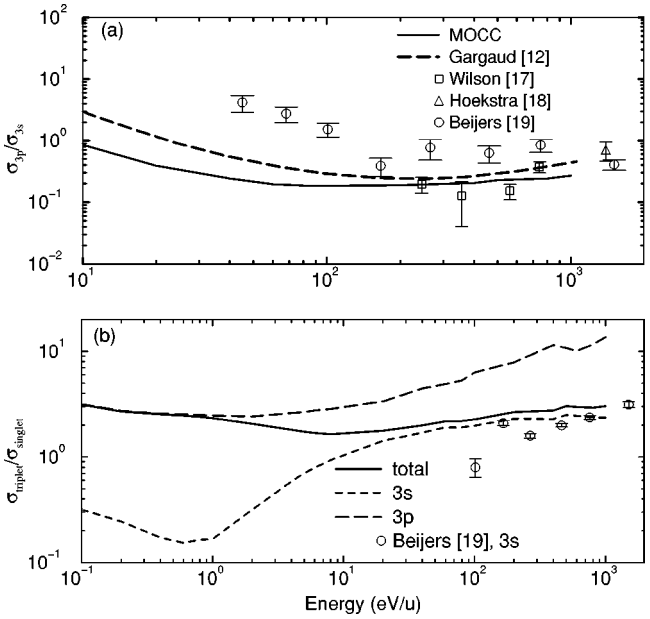

FIG. 6. The ratios of state-selective cross sections. (a) Capture to $O^{2+}(2p3p)$ and $O^{2+}(2p3s)$. Theory: present calculation (—), Gargaud *et al.* [12] (- -). Experiment: Wilson *et al.* [17] (open squares), Hoekstra *et al.* [18] (open triangles up), ''corrected'' Beijers *et al.* [19] (open circles). (b) Triplet-singlet cross section ratios: total SEC cross section (—), 3*s* state (- -), 3*p* state (—), measurement for capture to the 3*s* state [19] (open circle).

channels are found to be diabatic with avoided crossing distances of $\sim 19.7a_0$ and $\sim 17.8a_0$, respectively [21,34]. Examination of the OH_2^{3+} potential surfaces reveal no short-range, endoergic avoided crossings for $R_x \gtrsim 5$, indicating that possible crossings would have effective thresholds of at least 7 eV/u. This suggests, contrary to the PES measurements, that state-selective cross sections for capture to the $2p3p$ configuration should be small. On the other hand, avoided

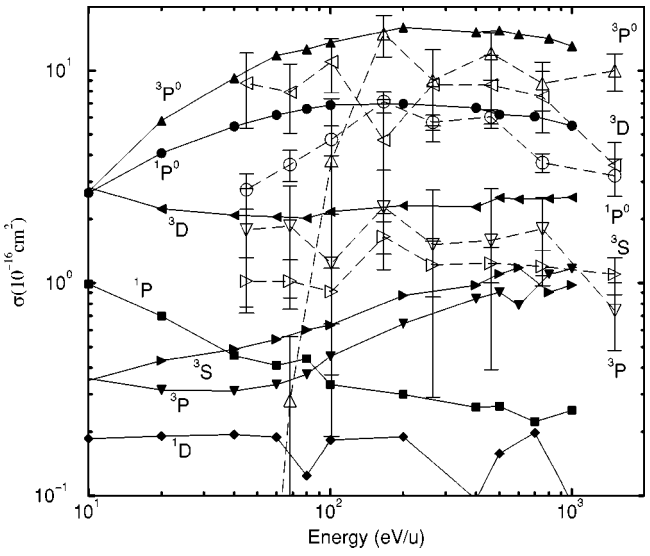

FIG. 7. MOCC state-selective cross sections for capture to different *LS* terms of $O^{2+}(2p3l)$. Present theory: lines with filled symbols; ''corrected'' experiment [19]: lines with open symbols.

crossings for the $2p3s$ states are in optimal locations between $R_x \sim 8a_0$ and $11a_0$, indicating significant cross sections, in harmony with experiment. Considering that there is a significant metastable population in the ion beam, it is worth considering what contribution it might make to the PES spectra. Given that the metastable state is a quartet, only triplet O^{2+} ions will be generated so that the singlets are completely unaffected by the presence of the metastable state. We have estimated the avoided crossing distances for $O^{3+}(2s2p^2\ ^4P)$ collisions with H_2 into O^{2+} triplet states to be $\sim 4a_0\ (2p3s)$, $\sim 5a_0\ (2p3p)$, $\sim (7-7.5)a_0\ (2p3d)$, $\sim 13a_0\ (2p4s)$, and $\sim 20a_0\ (2p4p)$. It therefore seems likely that the PES measurement for the triplet $2p3p$ states for the neutral H_2 beam is due to the O^{3+} metastable state, via either direct charge transfer or cascade from the $2p3d$ and $2p4s$ states with little contribution from the O^{3+} ground state. Further, the PES signal due to the $2p3s\ ^3P^o$ is also affected by cascades resulting from capture due to the metastable state, although it is probably dominated by direct capture from the O^{3+} ground state, it being the primary channel [21,34]. This implies that subtraction of the triplet spectrum due to H_2 from the composite H-H_2 spectrum results in an erroneous triplet H spectrum, and therefore triplet state-selective cross sections of unknown reliability, particularly for the $2p3p$ states, but less so for $2p3s\ ^3P^o$. The situation is further complicated by captures through metastable collisions with H which have avoided crossings of $\lesssim 4a_0\ (2p3p)$, $\sim 6a_0\ (2p3d)$, $\sim 9a_0\ (2p4s)$, and $\sim (11-12)a_0\ (2p4p)$ indicating that, while direct capture is probably not important, cascade contributions are. Therefore, while we do compare to the ''corrected'' (via branching ratios) PES measurements in Figs. 5–7, it may not be particularly useful when the triplet states are involved. Fortunately, while the TES measurements do have problems of metastable ion beam contamination and undissociated H_2, they are more easily separated out in energy-change spectra.

Keeping the concerns about the PES measurements discussed above in mind, we see in Fig. 5 that the present $2p3p$ MOCC cross section as well as that of Gargaud *et al.* are much smaller than the measurement of Beijers *et al.* On the other hand, the current results are in good agreement with both the measurements of Hoekstra *et al.* [18] and the TES results of Wilson *et al.* [17], where in the latter case we have normalized the relative experimental cross sections to our total MOCC cross section.

The agreement between experiment and theory is improved for the $2p3s$ configuration. The measurements of Wilson *et al.* and Hoekstra *et al.* are both consistent with the current MOCC calculations, while the Beijers *et al.* result is in agreement for $E \geqslant 166$ eV/u. For smaller energies, the discrepancy is due to the sudden drop of the $2p3s\ ^3P^o$ cross section which may be related to the complications of the metastable contamination.

In Fig. 6(a), the cross section ratio $(2p3p/2p3s)$ is plotted. The Beijers *et al.* measurement [19] appears to overestimate the ratio when compared to the experiment results of Wilson *et al.* and Hoekstra *et al.* and the current calculations and those of Gargaud *et al.*, giving further indications of difficulties in the former experiments.

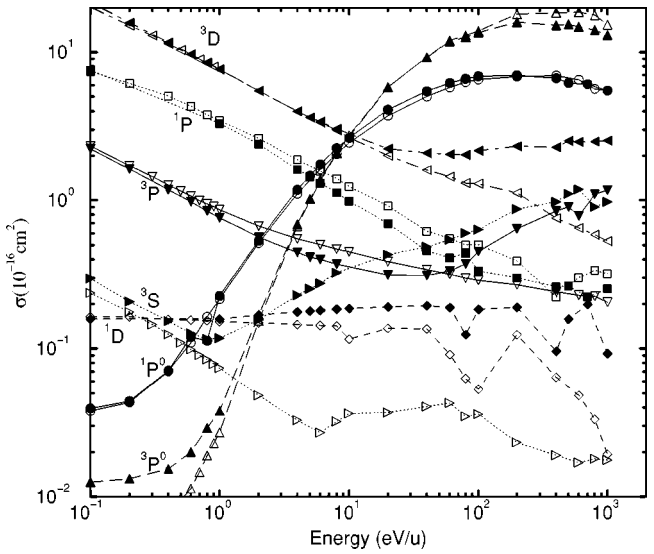

FIG. 8. MOCC state-selective cross sections with and without rotational coupling. With rotational coupling: lines with filled symbols; without rotational coupling: lines with open symbols.

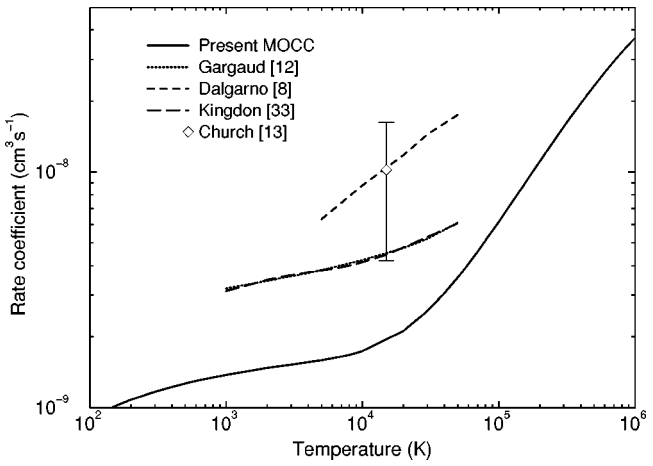

FIG. 9. Total SEC rate coefficients. Theory: present MOCC (—), Gargaud *et al.* [12] (···), Dalgarno *et al.* [8] (- -), Kingdon and Ferland [33] (– –); experiment: Church and Holzscheiter [13] (open diamonds).

In some astrophysical models, in particular that due to x-ray emission following charge transfer [35–37], the resulting population within triplet and singlet states is assumed to be according to spin statistics (i.e., 3:1), because of the lack of experimental and theoretical data. Ratios of triplet to singlet cross sections for $O^{3+}+H$ are plotted in Fig. 6(b). The ratio for the total cross section is in general agreement with the statistical value to within 30%. However, for capture to the $2p3s$ and $2p3p$ configurations, the simple statistical treatment is shown to fail, a trend that was noted previously for collisions of N^{4+} with H [38,39]. For the $2p3s$ configuration, the ratio falls below the statistical value as the energy decreases, in general agreement with the PES measurement of Beijers *et al.*, although the discrepancy in the lowest-energy point at 101 eV/u is again related to metastable contamination. This behavior is a consequence of the dependence of low-energy state-selective charge transfer cross sections on the detailed quasimolecular structure of the collision system. Surprisingly, the departure from the statistical value increases with energy for the $2p3p$ configuration. The current calculations suggest that the assumption of a statistical triplet-singlet ratio could introduce an error of a factor of a few to an order of magnitude in emission models.

LS-resolved state-selective cross sections for capture to $O^{2+}(2p3s\ ^1P^o,^3P^o)$ and $O^{2+}(2p3p\ ^1P,^1D,^3S,^3P,^3D)$ are shown in Figs. 7 and 8 with comparison to the measurements of Beijers *et al.* [19] given in the former. The cross section for capture to $O^{2+}(2p3p\ ^1S)$ was not computed as it was treated diabatically because its long-range avoided crossing $(23.09a_0)$ is extremely sharp as discussed in Sec. II. The current MOCC cross sections for capture to $O^{2+}(2p3s\ ^1P^o,^3P^o)$ are generally larger than experiment, while the calculations for capture to $O^{2+}(2p3p\ ^3S,^3P,^3D)$ are significantly smaller, being consistent with the results given in Fig. 4. As stated earlier, the discrepancy for the triplet $2p3p$ states and the $2p3s\ ^3P^o$ term is likely related to the metastable contamination of the experimental ion beam and the procedures used to deduce the state-selective cross sections. The one encouraging point is the reasonable agreement for the $2p3s\ ^1P^o$ state which is the only one believed not affected by the metastable.

Due to the limited detector wavelength range, Beijers *et al.* [19] were not able to measure the PES spectra for captures to $O^{2+}(2p3p\ ^1S,^1P,^1D)$. However, in the earlier experiment of Hoekstra *et al.* [18], the authors obtained cross section upper limits of 0.8×10^{-16} cm^2 for $O^{2+}(2p3p\ ^1P)$ and 0.5×10^{-16} cm^2 for $O^{2+}(2p3p\ ^1S,^1D)$ at a collision energy of 1.5 keV/u. These upper limits are consistent with the current calculations.

The state-selective cross sections are extended to lower energies in Fig. 8. For $E<2$ eV/u captures to $O^{2+}(2p3p\ ^3P,^1P,^3P)$ dominate while at higher energy (>20 eV/u) $O^{2+}(2p3s\ ^1P^o,^3P^o)$ are the most important. Comparison of the cross sections with and without rotational

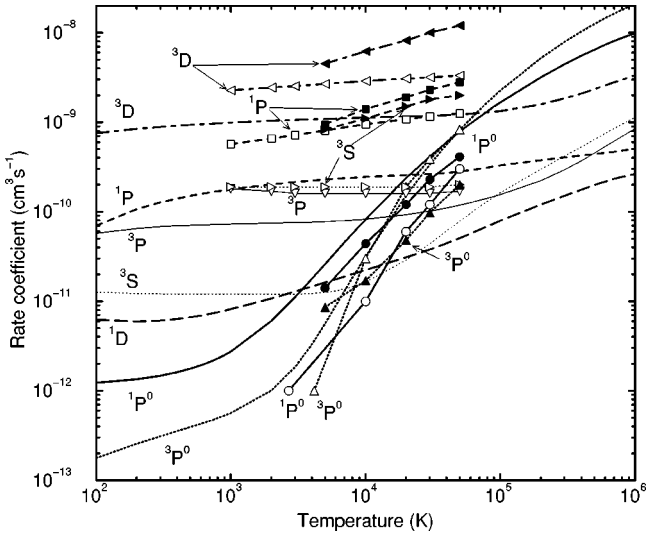

FIG. 10. State-selective SEC rate coefficients. Present MOCC calculations (lines without symbols), Gargaud *et al.* [12] (lines with open symbols), Dalgarno *et al.* [8] (lines with filled symbols).

TABLE IV. MOCC SEC rate coefficients α ($cm^3\ s^{-1}$) for $O^{3+}+H$ as a function of temperature T. Fitting parameters a_i($cm^3\ s^{-1}$), b_i, and c_i (K) for the relation $\alpha(T)=\Sigma_i a_i(T/10\ 000)^{b_i}\exp(-T/c_i)$ are given at the end of the table. (Numbers in square brackets denote powers of 10.)

T (K)	$3s\ ^1P^o$	$3s\ ^3P^o$	$3s$	$3p\ ^1P$	$3p\ ^1D$	$3p\ ^3S$	$3p\ ^3P$	$3p\ ^3D$	$3p$	Total
100	1.23[−12]	1.77[−13]	1.41[−12]	1.11[−10]	1.02[−11]	1.83[−11]	5.73[−11]	7.51[−10]	9.49[−10]	9.50[−10]
200	1.34[−12]	2.58[−13]	1.60[−12]	1.74[−10]	9.54[−12]	1.78[−11]	6.58[−11]	8.39[−10]	1.11[−09]	1.11[−09]
400	1.54[−12]	3.70[−13]	1.91[−12]	2.38[−10]	9.15[−12]	1.69[−11]	7.54[−11]	9.02[−10]	1.24[−09]	1.24[−09]
600	1.75[−12]	4.64[−13]	2.22[−12]	2.77[−10]	9.12[−12]	1.60[−11]	8.25[−11]	9.25[−10]	1.31[−09]	1.31[−09]
800	2.01[−12]	5.50[−13]	2.56[−12]	3.03[−10]	9.43[−12]	1.53[−11]	8.73[−11]	9.39[−10]	1.35[−09]	1.35[−09]
1000	2.33[−12]	6.34[−13]	2.96[−12]	3.23[−10]	9.89[−12]	1.48[−11]	9.06[−11]	9.50[−10]	1.39[−09]	1.39[−09]
2000	5.05[−12]	1.15[−12]	6.20[−12]	3.76[−10]	1.24[−11]	1.40[−11]	9.80[−11]	9.83[−10]	1.48[−09]	1.49[−09]
4000	1.55[−11]	3.55[−12]	1.90[−11]	4.16[−10]	1.64[−11]	1.50[−11]	1.02[−10]	1.02[−09]	1.57[−09]	1.58[−09]
6000	3.11[−11]	9.06[−12]	4.02[−11]	4.33[−10]	1.97[−11]	1.74[−11]	1.04[−10]	1.03[−09]	1.61[−09]	1.65[−09]
8000	5.08[−11]	1.83[−11]	6.91[−11]	4.41[−10]	2.27[−11]	2.06[−11]	1.06[−10]	1.05[−09]	1.64[−09]	1.70[−09]
10 000	7.35[−11]	3.15[−11]	1.05[−10]	4.46[−10]	2.54[−11]	2.41[−11]	1.08[−10]	1.05[−09]	1.66[−09]	1.76[−09]
20 000	2.17[−10]	1.49[−10]	3.66[−10]	4.52[−10]	3.68[−11]	4.42[−11]	1.16[−10]	1.09[−09]	1.74[−09]	2.10[−09]
40 000	5.64[−10]	5.60[−10]	1.12[−09]	4.48[−10]	5.39[−11]	8.44[−11]	1.30[−10]	1.14[−09]	1.86[−09]	2.98[−09]
60 000	9.28[−10]	1.09[−09]	2.01[−09]	4.44[−10]	6.72[−11]	1.21[−10]	1.43[−10]	1.19[−09]	1.96[−09]	3.98[−09]
80 000	1.28[−09]	1.66[−09]	2.94[−09]	4.41[−10]	7.85[−11]	1.53[−10]	1.55[−10]	1.24[−09]	2.07[−09]	5.01[−09]
100 000	1.63[−09]	2.25[−09]	3.88[−09]	4.38[−10]	8.83[−11]	1.83[−10]	1.67[−10]	1.29[−09]	2.17[−09]	6.04[−09]
200 000	3.16[−09]	5.19[−09]	8.36[−09]	4.34[−10]	1.25[−10]	3.11[−10]	2.27[−10]	1.56[−09]	2.66[−09]	1.10[−08]
400 000	5.52[−09]	1.03[−08]	1.59[−08]	4.48[−10]	1.79[−10]	5.36[−10]	3.74[−10]	2.09[−09]	3.62[−09]	1.95[−08]
600 000	7.30[−09]	1.45[−08]	2.18[−08]	4.68[−10]	2.19[−10]	7.50[−10]	5.34[−10]	2.56[−09]	4.53[−09]	2.64[−08]
800 000	8.72[−09]	1.80[−08]	2.67[−08]	4.90[−10]	2.46[−10]	9.50[−10]	6.94[−10]	2.98[−09]	5.35[−09]	3.21[−08]
1000 000	9.90[−09]	2.09[−08]	3.08[−08]	5.13[−10]	2.64[−10]	1.14[−09]	8.49[−10]	3.36[−09]	6.11[−09]	3.69[−08]
a_1	6.52[−11]	2.38[−11]	9.53[−11]	4.30[−10]	2.59[−11]	2.51[−11]	1.10[−10]	8.82[−10]	1.37[−9]	8.88[−10]
b_1	1.48	2.21	1.75	1.42[−2]	5.36[−1]	8.61[−1]	1.13[−1]	1.52[−1]	1.85[−1]	8.51[−1]
c_1	4.78[5]	2.12[5]	3.40[5]	−1.37[7]	7.79[6]	5.44[6]	−6.30[5]	−1.46[6]	−1.46[6]	5.66[6]
a_2	1.77[−12]	1.87[−12]	1.61[−12]	−1.09[−10]	2.56[−12]	1.98[−11]	−2.97[−11]	5.25[−10]	9.66[−10]	2.14[−9]
b_2	6.18[−1]	5.43[−1]	3.80[−1]	−2.21[−1]	−2.65[−1]	2.06[−2]	−8.46[−2]	1.23[−1]	2.20[−1]	1.84[−1]
c_2	7.79[2]	−1.49[5]	−1.09[5]	1.61[3]	1.14[3]	2.14[3]	5.79[1]	7.56[3]	7.24[3]	1.06[4]

coupling is also shown in Fig. 8. Inclusion of rotational coupling generally results in an increase in the cross sections of the $2p3p$ triplet states and particularly at the higher collision energies. The effect of rotational coupling is less pronounced for the $2p3s$ and the singlet $2p3p$ states. Enhancements due to rotational coupling appear to increase with increasing avoided crossing distances.

C. Rate coefficients

Rate coefficients were computed by extending the cross sections calculations to lower energy (0.1 meV/u) and averaging the cross sections over a Maxwellian velocity distribution. Total rate coefficients are plotted in Fig. 9. Comparison with other calculations [8,12] and one experimental point [13] shows the current results to be smaller by a factor of ~ 2. This discrepancy is a direct reflection of the differences noted for the total cross sections displayed in Fig. 4. As our total cross section is in close agreement with the merged-beams measurements [15,16], the current rate coefficients are expected to be the most reliable to date. Currently, most astrophysical photoionization models use the recommended rate coefficient fit of Kingdon and Ferland [33] which is based on the Gargaud *et al.* [12] calculation.

Figure 10 shows LS-resolved state-selective rate coefficients for capture to $O^{2+}(2p3s\ ^1P^o,^3P^o)$ and $O^{2+}(2p3p\ ^1P,^1D,^3S,^3P,^3D)$. The current results are found to be smaller than the calculations of Gargaud *et al.* [12] and Dalgarno *et al.* [8] for all of the $2p3p$ states, but generally larger for the $2p3s$ states. It is difficult to estimate the accuracy of our results in light of the complexities in the LS-resolved state-selective cross section measurments of Beijers *et al.* [19], but given that the current configuration-resolved cross sections are in best agreement with the measurements of Wilson *et al.* [17], we would expect the present LS-resolved rate coefficients to be the most reliable. Some numerical data and fits to these rate coefficients are presented in Table IV. The fits do not deviate from the computed rate coefficients by more than 20% for $10<T<10^6$ K, except for the $2p3p\ ^1P$ where the fit is only valid for $T>50$ K. For the $2p3s$ states the maximum deviation is $\sim 30\%$ for $T>700$ K, but worse for smaller T although the rate coefficients become small.

Fine-structure-resolved rate coefficients will be calculated in the future. It would be preferable to resolve the discrepancies between experiment and theory for the LS-resolved cross sections before hand. In the mean time, fine-structure-

resolved rate coefficients can be estimated by multiplying the current MOCC LS-resolved rate coefficients by the J-resolved cross section ratios for ^3D_J and ^3P_J calculated by Roueff and Dalgarno [11]. Roueff and Dalgarno noted that the ratios did not differ significantly from statistical values (i.e., $2J+1$).

V. SUMMARY

Quantum-mechanical MOCC calculations have been presented for electron capture following O^{3+} collisions with H over the energy range from 0.1 eV/u to 1 keV/u. Total and state-selective cross sections and rate coefficients are presented. Comparison with the existing experimental and theoretical data shows our total and configuration-resolved ($2p3s$ and $2p3p$) cross sections to be in better agreement with the experimental results than previous calculations. However, there are significant differences between our LS-resolved state-selective cross sections and the measurements of Beijers *et al.* [19] which we suggest are due to a combination of metastable contamination of the experimental ion beam and partial dissociation of the neutral hydrogen beam. New state-selective measurements are needed to sort out the discrepancies. Our calculations also show that rotational coupling is not important for the total cross section, at least for $E \lesssim 1$ keV/u, but that its contribution increases with energy for state-selective cross sections, particularly at the LS-resolved level.

ACKNOWLEDGMENTS

J.G.W. and P.C.S. acknowledge support from NASA Grants No. NAG5-9088 and No. NAG5-11453. We thank Bernard Zygelman for use of his MOCC code.

[1] I. Bowen, Publ. Astron. Soc. Pac. **46**, 146 (1934).
[2] I. Bowen, Astrophys. J. **81**, 1 (1935).
[3] J. E. McClintock, C. R. Canizares, and C. B. Tarter, Astrophys. J. **198**, 641 (1975).
[4] J. B. Oke and J. L. Greenstein, Astrophys. J. **211**, 872 (1977).
[5] C. R. Canizares, J. E. McClintock, and J. Grindlay, Astrophys. J. Lett. **236**, L55 (1980).
[6] C. R. Canizares, J. E. McClintock, and J. Grindlay, Astrophys. J. **234**, 556 (1979).
[7] S. E. Butler, T. G. Heil, and A. Dalgarno, Astrophys. J. **241**, 442 (1980).
[8] A. Dalgarno, T. G. Heil, and S. E. Butler, Astrophys. J. **245**, 791 (1981).
[9] T. G. Heil, S. E. Butler, and A. Dalgarno, Phys. Rev. A **27**, 2365 (1983).
[10] S. Bienstock, T. G. Heil, and A. Dalgarno, Phys. Rev. A **27**, 2741 (1983).
[11] E. Roueff and A. Dalgarno, Phys. Rev. A **38**, 93 (1988).
[12] M. Gargaud, Ph.D. thesis, Université de Bordeaux I, Bordeaux, France, 1987; M. Gargaud, R. McCarroll, and L. Opradolce, Astron. Astrophys. **208**, 251 (1989).
[13] D. A. Church and H. M. Holzscheiter, Phys. Rev. Lett. **49**, 643 (1982).
[14] R. A. Phaneuf, I. Alvarez, F. W. Meyer, and D. H. Crandall, Phys. Rev. **26**, 1892 (1982).
[15] C. C. Havener, M. P. Nesnidal, M. R. Porter, and R. A. Phaneuf, Nucl. Instrum. Methods Phys. Res. B **56/57**, 95 (1991).
[16] C. C. Havener, F. W. Meyer, and R. A. Phaneuf, in *Electronic and Atomic Collisions*, edited by W. R. MacGillivray, I. E. McCarthy, and M. C. Standage (IOP Publishing, Bristol, 1992), p. 381.
[17] S. M. Wilson, R. W. McCullough, and H. B. Gilbody, J. Phys. B **21**, 1027 (1988).
[18] R. Hoekstra, K. Boorsma, F. J. de Heer, and R. Morgenstern, J. Phys. (Paris), Colloq. **50**, 349 (1989).
[19] J. P. M. Beijers, R. Hoekstra, and R. Morgenstern, J. Phys. B **29**, 1397 (1996).
[20] D. L. Cooper, N. J. Clarke, P. C. Stancil, and B. Zygelman, Adv. Quantum Chem. **40**, 37 (2001).
[21] A. R. Turner, Ph.D. thesis, University of Liverpool, England, 2002.
[22] B. Zygelman, D. L. Cooper, M. J. Ford, A. Dalgarno, J. Gerratt, and M. Raimondi, Phys. Rev. A **46**, 3846 (1992).
[23] P. O. Löwdin, Phys. Rev. **97**, 1474 (1955).
[24] M. Kimura and N. F. Lane, Adv. At., Mol., Opt. Phys. **26**, 79 (1990).
[25] B. H. Bransden and M. R. C. McDowell, *Charge Exchange and the Theory of Ion-Atom Collisions* (Clarendon Press, Oxford, 1992).
[26] B. R. Johnson, J. Comput. Phys. **13**, 445 (1973).
[27] R. K. Janev, L. P. Presnyakov, and V. P. Shevelko, *Physics of Highly Charged Ions* (Springer-Verlag New York, 1985).
[28] L. F. Errea, C. Harel, H. Jouin, L. Méndez, B. Pons, and A. Riera, J. Phys. B **27**, 3603 (1994).
[29] P. C. Stancil and B. Zygelman, Phys. Rev. Lett. **75**, 1495 (1995).
[30] S. E. Butler and A. Dalgarno, Astrophys. J. **241**, 838 (1980).
[31] R. K. Janev, D. S. Belić, and B. H. Brandsen, Phys. Rev. **28**, 1293 (1983).
[32] W. L. Wiese, J. R. Fuhr, and T. M. Deters, J. Phys. Chem. Ref. Data Monograph **7**, 532 (1996).
[33] J. B. Kingdon and G. J. Ferland, Astrophys. J. Suppl. Ser. **106**, 205 (1996).
[34] J. G. Wang, P. C. Stancil, A. R. Turner, and D. L. Cooper (unpublished).
[35] P. Beiersdorfer, C. M. Lisse, R. E. Olson, G. V. Brown, and H. Chen, Astrophys. J. Lett. **549**, L147 (2001).
[36] B. J. Wargelin and J. J. Drake, Astrophys. J. Lett. **546**, L57 (2001).
[37] V. Kharchenko and A. Dalgarno, Astrophys. J. Lett. **554**, L99 (2001).
[38] F. W. Bliek, G. R. Woestenenk, R. Hoekstra, and R. Morgenstern, Phys. Rev. A **57**, 221 (1998).
[39] P. C. Stancil, B. Zygelman, N. J. Clarke, and D. L. Cooper, J. Phys. B **30**, 1013 (1997).
[40] NIST Atomic Spectra Database, Version 2.0, 1999, http://physics.nist.gov/asd.